ACS APPLIED NANO MATERIALS

www.acsanm.org Article

Vertically Oriented Carbon Nanotubes for Thermal Management

Jing Peng, Yang Zhou, Lifen Su,* Haoming Xie, Ru Xia, Bin Wu, Jiasheng Qian,* and Lei Miao*

Cite This: *ACS Appl. Nano Mater.* 2025, 8, 3219−3226 Read Online

ACCESS | Metrics & More | Article Recommendations | Supporting Information

ABSTRACT: Efficient heat dissipation is an important technology to address the issues of overheating and increasing heat flux density for high-density integrated electronic devices toward miniaturization, multifunctionality, and high integration. Carbon nanotubes (CNTs) are considered as an ideal thermally conductive filler of polymeric encapsulation owing to its excellent thermal conductivity and unique linear structure but suffer from the random arrangement in the composites and extremely low thermal conductivity of the polymeric matrix. Here, we report vertically aligned carbon nanotubes (VACNTs) grown in situ by chemical vapor deposition, which were modified by polyethylene polyamine and covered with poly(vinyl alcohol) (PVA) to form the *m*-VACNTs/PVA thermally conductive composite film. The out-of-plane thermal conductivity of the *m*-VACNTs/PVA film reaches as high as 14.9 W m^{-1} K^{-1}, which is approximately 53 times that of a pure PVA film. In addition, the *m*-VACNTs/PVA composites have excellent electrical conductivity and an outstanding electromagnetic shielding effect. This study provides a promising strategy for design of advanced composites with high thermal conductivity in the vertical direction.

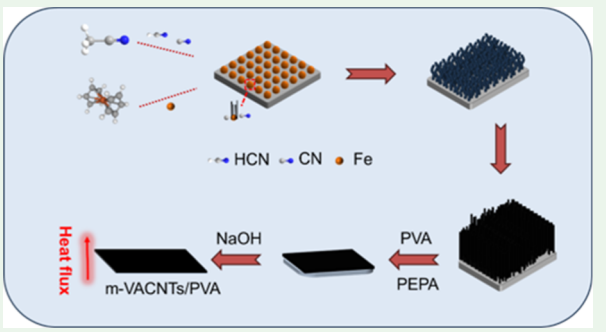

KEYWORDS: *CNTs, vertically aligned, thermal conductivity, electromagnetic shielding, electrical conductivity*

1. INTRODUCTION

The rapid development of electronic devices toward miniaturization, high power, and high integration inevitably gives rise to heat cumulation and an increase in heat density, which results in a decrease of service life and even failure for electronic devices.[1−4] Meanwhile, the part of heat generated by the released electromagnetic radiation via reflection and absorption also contributes to the overheating of a highly integrated microsystem.[5−7] Electromagnetic radiation pollution is avoided by absorbing electromagnetic energy and converting it into heat, which leads to an increase of temperature.[8,9] Therefore, it is an urgent need to develop a high-performance thermal management material with high thermal conductivity and excellent electromagnetic shielding for modern electronic devices.[10,11]

Thermal interface materials (TIMs) have emerged as critical components in the entire thermal design system of electronic devices. TIMs can eliminate the air gap between heat sources and heat sinks, substantially reducing thermal resistance and enhancing heat transfer efficiency.[12] Given the advantages of lightweight, deformability, excellent flexibility, and low-cost properties of polymers, TIMs are usually composites of polymeric matrices and highly thermally conductive fillers. However, polymers inherently have low thermal conductivity in the range of 0.1−0.5 W/(m·k).[13,14] It is a promising strategy to fill the thermally conductive fillers in the polymers to improve the thermal conductivity of TIMs. The outstanding thermally conductive fillers such as the two-dimensional (2D) (e.g., graphene, boron nitride (BN), and MXenes) and one-dimensional (1D) materials (e.g., carbon nanotubes (CNTs) and carbon fibers) have been widely investigated due to their high theoretical thermal conductivity.[12,15,16] Specially, the CNTs exhibit excellent electrical conductivity, flexibility, and high aspect ratios, which endow extremely high thermal conductivity exceeding 3000 W/(m·K) theoretically and are deemed as one of the most promising candidates for thermally conductive and electrical applications.[17−21] However, the CNTs-based composites obtained by simply mixing CNTs and polymers usually have a lower thermal conductivity due to the failed construction of CNTs into effective thermally conductive pathways. Recently, many efforts have been made to improve the thermal conductivity of polymeric encapsulation materials. Li et al. utilized an ice templating method to form the oriented ZIF-67 and then derived CNTs in situ as a 3D thermal conductivity network,[22] and the composite showed a high thermal conductivity of 0.98 W/(m·K) after filling with epoxy. Yang et al. employed an electrostatic spinning method to construct a synergistic hybrid structure of CNTs bridging BNNSs along PVA fibers and then infused with epoxy[23] to

Received: December 18, 2024
Revised: January 24, 2025
Accepted: January 28, 2025
Published: February 3, 2025

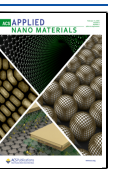

https://doi.org/10.1021/acsanm.4c07152
ACS Appl. Nano Mater. 2025, 8, 3219−3226

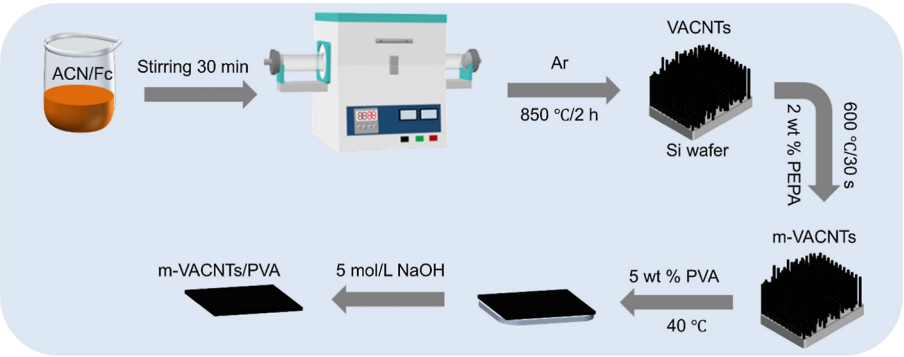

Figure 1. Schematic illustration of the preparation of oriented *m*-VACNTs/PVA composites.

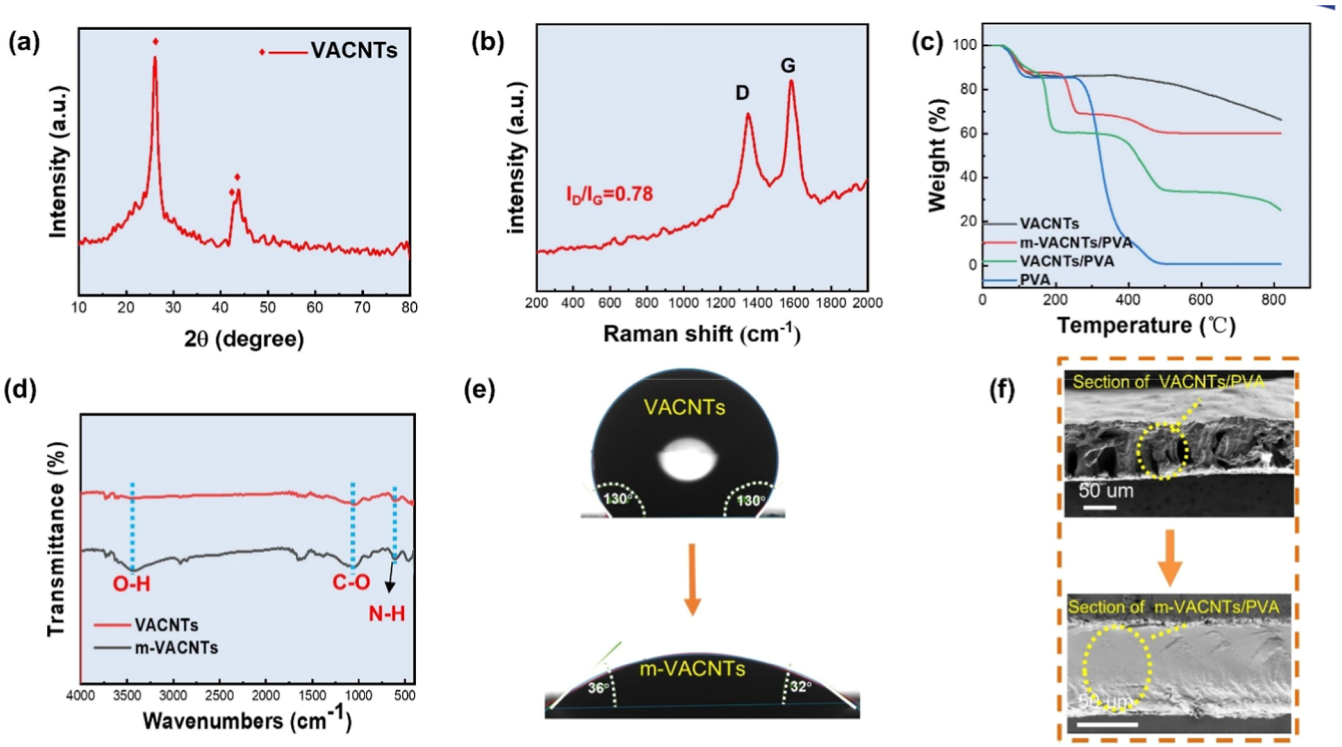

Figure 2. XRD pattern (a) and Raman spectroscopy (b) of VACNTs powder. (c) TGA curves of PVA, VACNTs, VACNTs/PVA, and *m*-VACNTs, respectively. (d) FT-IR spectra of VACNTs and *m*-VACNTs. (e) Contact angle measurement of VACNTs and *m*-VACNTs. (f) SEM images of cross sections of VACNTs/PVA and *m*-VACNTs/PVA, respectively.

obtain the epoxy/PVA (BNNSs/CNTs) composite film with a high in-plane thermal conductivity of 6.3 W/(m·K) at a total filler content of 27.5 wt %. Cai et al. grew vertically aligned CNTs on a quartz substrate by injecting precursors and passing hydrogen, and the prepared CNTs/silicone rubber exhibited a thermal conductivity of 4.3 W/(m·K).[24] Though these methods have improved the thermal conductivity of CNTs-based composites, the preparation calls for a large content of thermally conductive fillers, resulting in a complex and expensive process.

In this work, vertically aligned CNTs (VACNTs) were grown in situ by facile chemical vapor deposition (CVD) for a highly efficient thermally conductive film after filling with PVA. The obtained CNTs were highly dense and vertically oriented with lengths ranging from 40 to 70 μm. The CNTs were modified by polyethylene polyamine (PEPA) to enhance their hydrophilicity, resulting in excellent compatibility with the matrix of PVA via hydrogen bonding to fabricate the *m*-VACNTs/PVA composite films. The out-of-plane thermal conductivity of the *m*-VACNTs/PVA composite can reach 14.9 W/(m·K). Furthermore, the composites also exhibit a large alternating current conductivity of 0.6 S/cm. These findings provide a promising strategy for design of high-performance thermal conductive composites with the function of electromagnetic shielding in the field of electronic packaging.

2. EXPERIMENTAL SECTION

2.1. Materials. Acetonitrile (ACN, 99.9%), ferrocene (Fc, AR), and poly(vinyl alcohol) (PVA, D_P = 1788) were purchased from Aladdin Chemistry Co., Ltd. Sodium hydroxide and PEPA (98%) were obtained from Sinopharm Chemical Reagent and Shanghai Macklin Biochemical Technology Co., Ltd., respectively.

2.2. Growth of VACNTs. First, ACN and Fc were mixed with the weight ratio of 10:1 and stirred for 30 min in a beaker and then transferred into a crucible. Second, a cleaned silicon wafer (cleaning process in Supporting Information) was covered on the surface of the

https://doi.org/10.1021/acsanm.4c07152
ACS Appl. Nano Mater. 2025, 8, 3219−3226

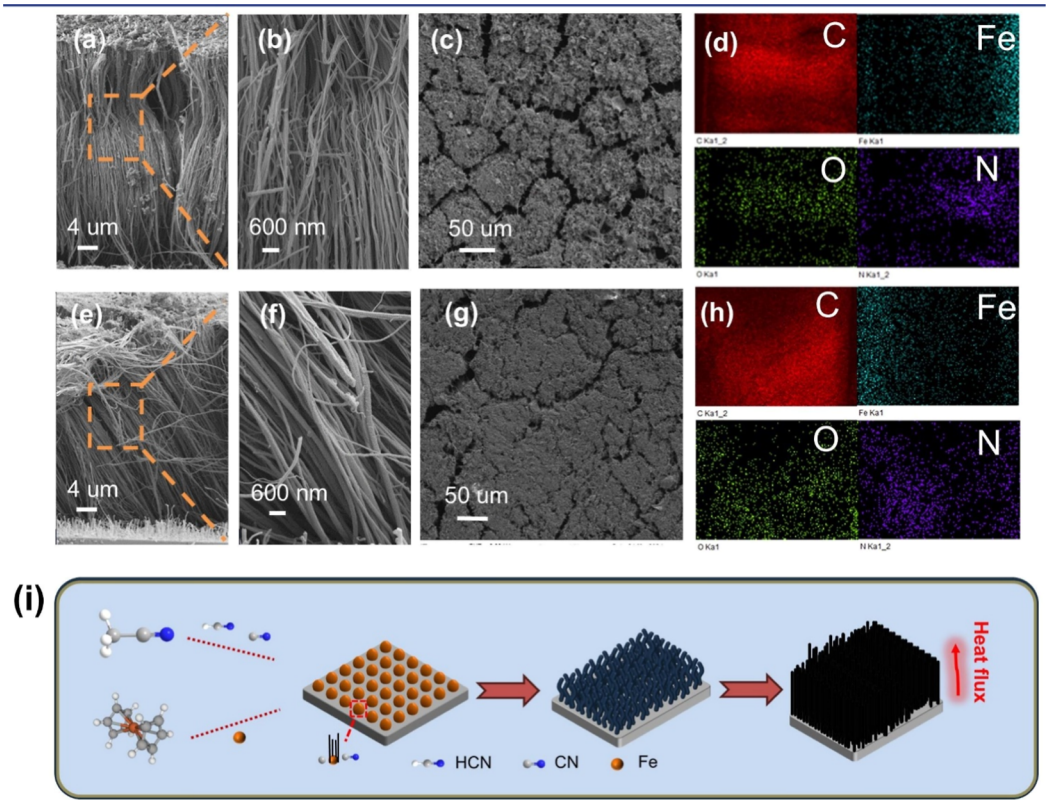

Figure 3. (a,b) Cross-section and (c) top-view SEM images of VACNTs. (e,f) Cross-section and (g) top-view SEM images of *m*-VACNTs. (d,h) Elemental mapping images of VACNTs and *m*-VACNTs, respectively. (i) Growth mechanism and thermal conduction pathway of VACNTs.

crucible completely, followed by transferring to a tube furnace for annealing. The ordered VACNTs were grown on a silicon wafer at 850 °C for 2 h with a heating rate of 5 °C/min under an atmosphere of argon.

2.3. Modification of VACNTs. The VACNTs on the wafers were immersed in the prepared 2 wt % PEPA solution for 10 min and then transferred to an infrared fast annealing furnace at 600 °C for 30 s. The samples were washed repeatedly with deionized water to obtain modified VACNTs (*m*-VACNTs).

2.4. Preparation of the *m*-VACNTs/PVA Film. The 5 wt % PVA solution was dropped onto the surface of VACNTs for uniform distribution, which was dried in an oven at 60 °C to form a *m*-VACNTs/PVA film with excellent mechanical property. Subsequently, the substrate of silicon wafer was corroded by immersing it in a NaOH solution (5 mol/L) at 50 °C, and the *m*-VACNTs/PVA film was stripped after etching for 2 h. Finally, the film was washed with ethanol and water repeatedly until the pH value of the solution was 7.

2.5. Characterization. The crystal structure of the sample was characterized by using an X-ray diffractometer (X′ Pert Pro MPD, PANalytical) with X-ray diffraction employing Cu Kα radiation (λ = 0.1541 nm) and a Raman spectrometer (inVia Reflex, Britain). The filler content in the composite was determined by thermogravimetric analysis (TGA, TG209F3, NETZSCH). The microscopic morphology was observed with a field-emission scanning electron microscope (FESEM, Regulus 8200, Hitachi) and a transmission electron microscope (JEM-2100F, Japan), respectively. The changes of sample before and after modification were tested by using a contact angle device (DSA30S, Krüss) and Fourier transform infrared spectrometer (FT-IR, Nicolet is50, America). The surface temperature changes were captured with an infrared camera (T1040, FLIR). Alternating current conductivity at different frequencies was recorded with a broadband dielectric impedance spectrometer (Novocontrol Concept 40, Germany). The thermal diffusivity (α) of the films was measured via a laser flash apparatus (LFA467, China), and the corresponding thermal conductivity (k) was calculated by the formula $k = \alpha\rho C_p$, where ρ is the density and C_p is the specific heat capacity. The C_p was determined by a NETZSCH thermal analyzer (STA 449F3, NETZSCH), and the density (ρ) was calculated using the formula $\rho = m/v$, where m is the weight and v is the volume, respectively.

3. RESULTS AND DISCUSSION

The preparation of oriented *m*-VACNTs/PVA composites is illustrated in Figure 1, and the mixture of ACN/Fc was covered by a clean silicon wafer and annealed in a tube furnace for in situ growth of VACNTs via CVD. After cooling, a large number of VACNTs were grown on the surface of silicon wafer neatly. To the best of our knowledge, the gaps between the vertically arranged CNTs will form the interfacial thermal resistance in the composites, leading to a decrease in the thermal conductivity greatly, which should be avoided or narrowed. Here, the VACNTs were modified by soaking in PEPA solution and followed by rapid infrared annealing to improve the compatibility between the fillers and matrix of PVA. Owing to the advantages of transparent and outstanding mechanical property, PVA solution was dropped onto the *m*-VACNTs to form the tight *m*-VACNTs/PVA composite film. The Si substrate was etched by immersing in a NaOH solution, and the desired *m*-VACNTs/PVA film was obtained for thermal conductivity.

The structure of the grown VACNTs was characterized through XRD and Raman spectroscopy (Figure 2a,b). Obviously, a distinct diffraction peak at 26° corresponds to the (002) plane of graphite carbon, and the peaks at 42° and 44° are attributed to the (100) and (101) planes of CNTs, respectively, demonstrating a well-established graphite structure. Raman spectroscopy shows that the I_D/I_G ratio of VACNTs is 0.78, indicating that the in situ growth of

https://doi.org/10.1021/acsanm.4c07152
ACS Appl. Nano Mater. 2025, 8, 3219−3226

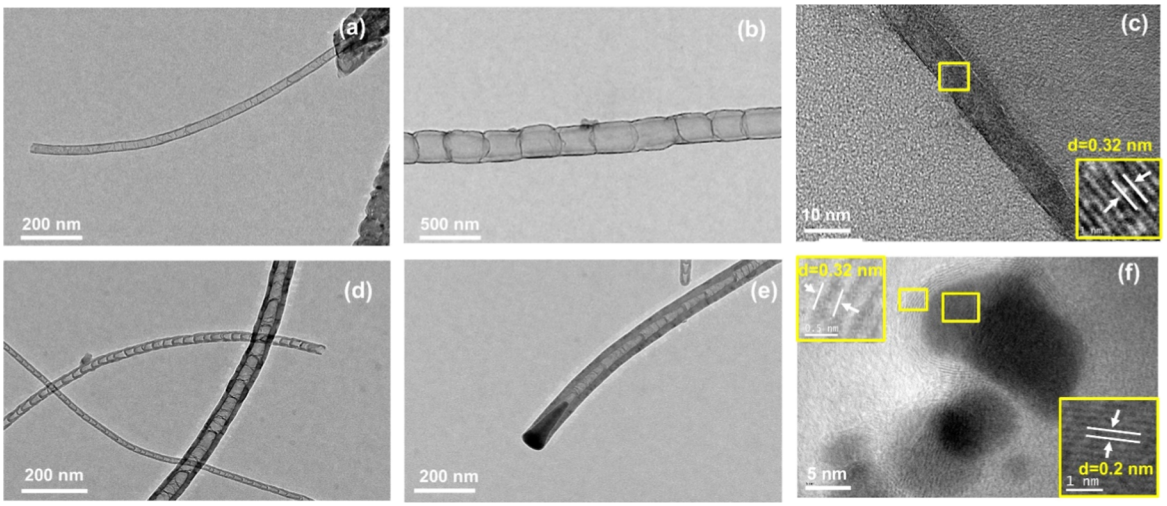

Figure 4. TEM (a,b) and HRTEM (c) images of VACNTs. TEM (d,e) and HRTEM (f) images of *m*-VACNTs modified with PEPA.

VACNTs has a higher degree of graphitization with few defects. The thermal decompositions of VACNTs/PVA and *m*-VACNTs/PVA from 40 to 800 °C are shown in Figure 2c. The first stage of weight loss mainly involves the removal of water, and the second stage is due to the decomposition of the PVA macromolecular chain into small fragments. The thermal decomposition of *m*-VACNTs/PVA occurs at a higher temperature compared to that of VACNTs/PVA, which can be attributed to the PEPA modification with grafted groups to form stable hydrogen bonds.

The FT-IR spectra of the VACNTs before and after modification are shown in Figure 2d. For *m*-VACNTs, the broad peak at 3500 cm^{-1} is significantly enhanced, which is attributed to the stretching vibration of the O−H bond, demonstrating the improved hydrophilicity of the composites. The enhancement of the bending vibration peak of the amide N−H at 1700 cm^{-1} and the stretching vibration peak of C−O at 1100 cm^{-1} suggests that the functional groups of PEPA were successfully grafted to the surface of VACNTs during the modification process. As shown in Figure 2e, the contact angle of the *m*-VACNTs/PVA composite is 35.5°, which is much lower than that of VACNTs PVA without modification, indicating that the PEPA can improve the hydrophilicity of VACNTs effectively and reinforce the compatibility between fillers and PVA to form the high thermal conductivity composites.

These results are in good agreement with the FT-IR and SEM images. The cross-sectional SEM images of the films before and after modification are shown in Figure 2f. Obviously, the modified *m*-VACNTs/PVA film exhibits an excellent interfacial compatibility without gaps by contrast to that of the original VACNTs/PVA film, implying the modification of PEPA is an efficient way to decrease the interfacial heat resistance of composites.

The cross-sectional SEM images of the VACNTs before and after modification with PEPA are shown in Figure 3. For the VACNTs, it can be observed that a large number of nanotubes with the length of 40−70 μm grow neatly vertically on the substrate (Figure 3a,b), and the top view image (Figure 3c) shows the CNTs are grown in clusters, and gaps between clusters are 1−5 μm. The elemental mapping images of VACNTs (Figure 3d) show that the C, O, and N elements are distributed uniformly, and the Fe atoms are mainly located at the tips of the nanotubes. Such large gaps in the VACNTs film are not conducive to thermal conduction, which were modified with PEPA. It can be seen that the VACNTs incline on the substrate with uniform dispersion and a smooth top view image (Figure 3e−g). Besides, the EDS images (Figure S1) show that the atom ratios of C, N, O, and Fe for VACNTs are 93, 5, 1, and 1%, respectively, indicating few impurities in the sample. The increased N and O content of *m*-VACNTs also confirms the successful modification by PEPA. The growth mechanism of vertically aligned CNTs can be ascribed to both tip growth and segmented growth as shown in Figure 3i. Initially, the Fc was decomposed into Fe and C particles, and acetonitrile was disassembled into CN and HCN molecules at a high temperature under an argon atmosphere. The Fe particles adhere to the surface of silicon wafer and work as nucleation seeds for growth of CNTs. The C and CN are absorbed by the roots of Fe particles, and the cumulated C and CN particles pressure on the Fe particles to elongate and facilitate the formation of random short nanotubes (Figure 3e). The growth density of the CNTs increases with the increasing random short nanotubes (Figure 3e) and density of Fe particles until steady-state equilibrium; then the nanotubes grow tightly in the vertical direction, extending section by section via the segmented growth method. Interestingly, the Fe atoms are always sealed at the tips of nanotubes, which has been demonstrated by the mapping images of Fe elements in Figure 3d,h. For order-aligned polymer-based thermal conductive composites, the thermal conductivity mainly depends on the mobility of phonons via the ordered pathway. Vertically aligned CNTs allow phonons transport in the vertical direction and thus faster heat transfer.[25−31]

The high-resolution transmission electron microscopy (HRTEM) images of VACNTs and *m*-VACNTs are shown in Figure 4. Notably, the diameters of VACNTs are in the range of 40−200 nm, indicating the length−diameter ratio is as large as 1750:1 according to the length in the SEM image (Figure 3b). Specially, the CNTs are composed of numerous segments like bamboo joints section by section with ultrathin walls (Figure 4b). Moreover, Figure 4e shows that the Fe atom is squeezed and sealed in the tips of nanotubes, which works as a nucleation center of the nanotube and facilitates the nanotube growing section by section, verifying the growth mechanism of VACNTs in Figure 3i. After modification with

https://doi.org/10.1021/acsanm.4c07152
ACS Appl. Nano Mater. 2025, 8, 3219−3226

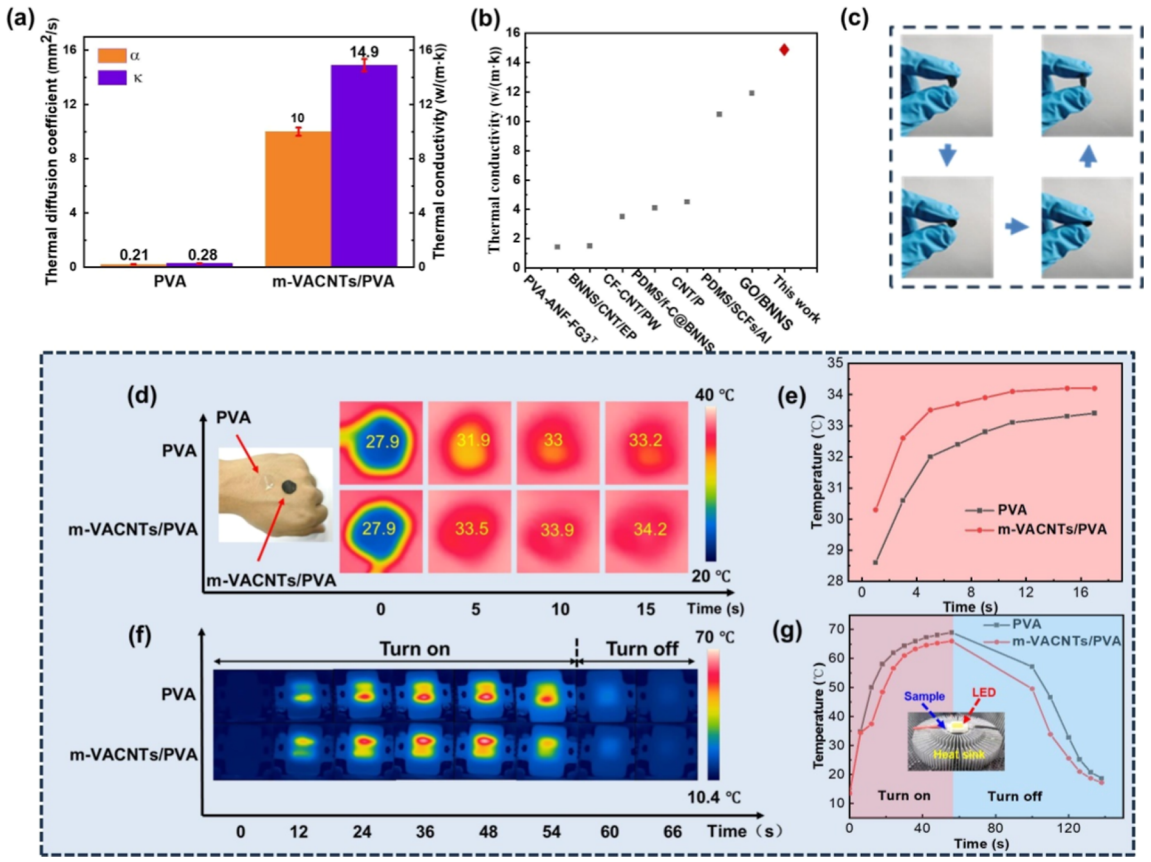

Figure 5. (a) Thermal diffusivity and thermal conductivity of PVA and *m*-VACNTs/PVA films. (b) Comparison of thermal conductivities between reported oriented composites and this work.[24,32−37] (c) Flexibility measurement of the *m*-VACNTs/PVA film. (d) PVA and *m*-VACNTs/PVA were placed on a fist, and the infrared temperature images change with time; (e) corresponding curves of temperature variation. (f) Infrared temperature images of the LED chip with time by placing the samples into the interface between the LED chip and heat sink, and (g) corresponding temperature curves, where the chip was lit for 54 s and then turned off.

PEPA, the surface of *m*-VACNTs was covered with a uniform organic layer (Figure 4d), indicating that the functional groups of PEPA have been successfully grafted onto the surface of VACNTs. HRTEM images (Figure 4c) show that the lattice spacing of 0.32 nm is assigned to the (002) plane of graphitic carbon, which is in good agreement with the results of XRD in Figure 2a. For the *m*-VACNTs, the lattice spacing of 0.2 and 0.32 nm around the Fe atoms corresponds to the (101) and (002) crystal planes of graphitic carbon, respectively.

The thermal conductive performances of the *m*-VACNTs/PVA film are indicated in Figure 5. The thermal diffusivity of the *m*-VACNTs/PVA film is 10 mm^2/s, and the corresponding thermal conductivity is calculated as 14.9 W/(m·K), which is 53 times that of the PVA film (0.28 W/(m·K)). It can be because the order vertically aligned CNTs construct effective pathways for phonon transmission to obtain fast thermal diffusivity. By comparation, the out-of-plane thermal conductivity of *m*-VACNTs/PVA composites in this study (Figure 5b) is superior to those of reported thermally conductive composites filled with 1D and 2D fillers,[24,32−37] demonstrating that the construction of vertically aligned CNTs skeletons facilitates the heat transports between different planes in the longitudinal direction. As shown in Figure 5c, the flexible *m*-VACNTs/PVA film was bent and even folded, which can recover to its original morphology without any deformation after removing the external force, indicating the *m*-VACNTs/PVA film with excellent mechanical properties can be applied in the field of flexible electronic devices. For actual application of heat dissipation on a fist, the real-time temperature changes of PVA and the *m*-VACNTs/PVA films were captured by an infrared thermal imager (Figure 5d). It can be observed that the temperature of the *m*-VACNTs/PVA film increases to 33.5 °C in 5 s and then rises to 34.2 °C after 15 s, which is significantly higher than that of the PVA film (Figure 5e), suggesting excellent thermal conductivity of the *m*-VACNTs/PVA film. To evaluate the actual heat dissipation in the thermal management of electronic devices, the *m*-VACNTs/PVA film was used as a thermal interfacial material to replace thermal grease between LED chips and heat sinks. When the chip is turned on, the temperature of the chip with the *m*-VACNTs/PVA film increases to 65.4 °C at 54 s (Figure 5f,g), which is lower than that of the PVA film (69.6 °C), indicating that the *m*-VACNTs/PVA film can transport the heat energy to the bottom heat sink for heat dissipation effectively. When the power is turned off, the temperature of the chip with the *m*-VACNTs/PVA film decreases sharply but is always lower than that of the PVA film. This can be ascribed to the fact that the vertically aligned CNTs provide numerous thermal conductive pathways via each nanotube to facilitate the rapid transfer of heat flow from the bottom to the top, demonstrating an outstanding heat dissipation effect. Thus, the *m*-VACNTs/PVA composite has significant application potential in the interfacial thermal conductivity of electronic devices.

https://doi.org/10.1021/acsanm.4c07152
ACS Appl. Nano Mater. 2025, 8, 3219−3226

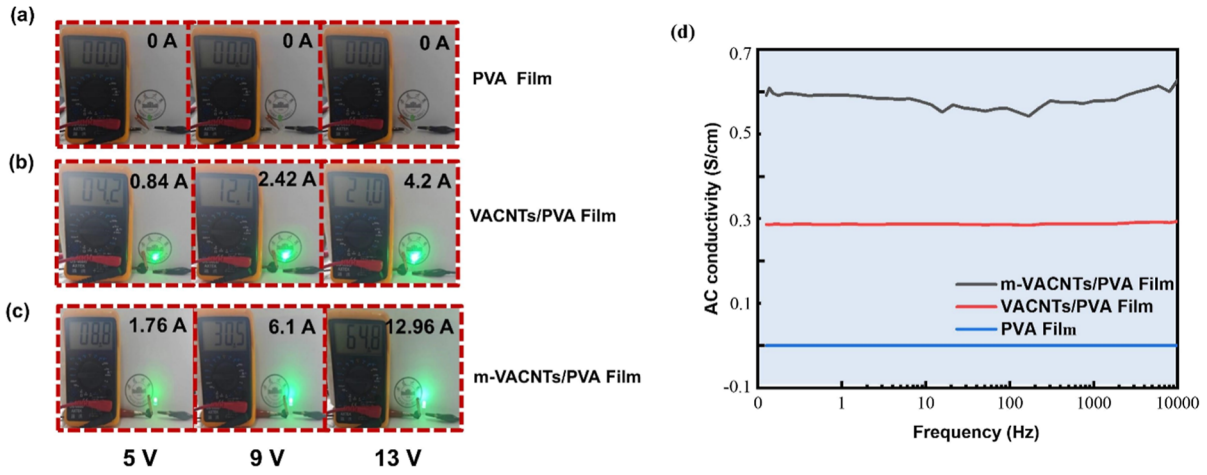

Figure 6. Electrical conductivity measurements of PVA (a), VACNTs/PVA (b), and *m*-VACNTs/PVA composites (c) by connecting a multimeter and LED light under a constant voltage of 5, 9, and 13 V, respectively. (d) AC conductivities of PVA, VACNTs/PVA, and *m*-VACNTs/EP composites with frequency.

The electrical conductivity was further investigated via a circuit with a multimeter, an LED light, and samples under a constant voltage of 5, 9, and 13 V (Figure 6a–c), respectively. Obviously, the LED light connecting with the PVA film cannot be lit, indicating electronic insulation. In contrast, the LED lights with VACNTs/PVA and *m*-VACNTs/PVA films light and become more and more brighter with an increase of voltage, and the electric current reading of the multimeter increases synchronously. By comparison with VACNTs/PVA, the LED light with *m*-VACNTs/PVA exhibits more lighter and larger current readings as 12.96 A (grade of 200 mA) at 13 V, which is about 4 times that of the VACNTs/PVA film, demonstrating superior electronic conductivity of the *m*-VACNTs/PVA composite. It can be ascribed to two factors which are as follows. On the one hand, the little doping nitrogen into CNTs (Figure 3d and h) during the growth process can generate additional electrons to form the electronic current, resulting in enhancement of the electronic conductivity of CNTs.[38] On the other hand, PEPA molecules react with CNTs to form stable interactions and improve electronic coupling between CNTs, leading to lower interfacial contact resistance between nanotubes and forming a more effective conductive network. Taking the actual application of alternating current (AC) into account, the AC conductivities of PVA, VACNTs/PVA, and *m*-VACNTs/PVA composites are further explored in the frequency range of 0–10000 Hz as shown in Figure 6d. The AC conductivity of the *m*-VACNTs/PVA composite is 0.6 S/cm, which is about 2 times that of VACNTs/PVA (0.28 S/cm), confirming the excellent electronic conductivities of VACNTs/PVA and *m*-VACNTs/PVA. Furthermore, the saturation magnetic induction of *m*-VACNTs is also stronger than that of VACNTs (Figure S2). Taking advantage of the excellent electrical conductivity and magnetic property of the *m*-VACNTs/PVA composite, the electromagnetic shielding performances of the composite films are further investigated in the frequency band from 8 to 12 GHz (Figure S3). For the *m*-VACNTs/PVA composite, the total shielding efficiency (SE_T) of electromagnetic interference (EMI) is more than 20 dB in the X band, and the electromagnetic absorbed loss (SE_A) is the most important electromagnetic shielding in comparison with the reflection loss (SE_R). These findings demonstrate the *m*-VACNTs/PVA composite not only has a large electronic conductivity but also exhibits an outstanding electromagnetic shielding capability, which provides a promising strategy for advanced interface thermal management materials.

4. CONCLUSIONS

In summary, we reported vertically aligned CNTs that were grown in situ on a silicon wafer by the CVD method with acetonitrile as the carbon source and ferrocene as a catalyst. The lengths of VACNTs are in the range of 40–70 μm with a large length–diameter ratio of 1750. The VACNTs modified with PEPA not only improve the hydrophilicity between fillers and PVA but also enhance the thermal and electronic conductivity of the composites. The thermal diffusivity and conductivity of the *m*-VACNTs/PVA composite can reach 10 mm^2/s and 14.9 W/(m·K), respectively. Furthermore, the *m*-VACNTs/PVA composite exhibits an excellent electromagnetic shielding capability. The *m*-VACNTs/PVA composite has promising applications in thermal management devices as well as electrical devices.

■ ASSOCIATED CONTENT

Supporting Information

The Supporting Information is available free of charge at https://pubs.acs.org/doi/10.1021/acsanm.4c07152.

EDS spectra of VACNTs and *m*-VACNTs, hysteresis loop of VACNTs and *m*-VACNTs, and EMI of PVA and *m*-VACNTs/PVA films in the X band (PDF)

■ AUTHOR INFORMATION

Corresponding Authors

Lifen Su – *School of Materials Science and Engineering, Anhui University, Hefei 230601, China; Key Laboratory of Environment-Friendly Polymeric Materials of Anhui Province, School of Chemistry and Chemical Engineering, Anhui University, Hefei 230601, China;* orcid.org/0000-0002-7667-3004; Email: ausulf@sina.com

Jiasheng Qian – *Key Laboratory of Environment-Friendly Polymeric Materials of Anhui Province, School of Chemistry and Chemical Engineering, Anhui University, Hefei 230601, China*; Email: qianjsh@ahu.edu.cn

https://doi.org/10.1021/acsanm.4c07152
ACS Appl. Nano Mater. 2025, 8, 3219–3226

Lei Miao − *Guangxi Key Laboratory for Relativity Astrophysics, State Key Laboratory of Featured Metal Materials and Life-cycle Safety for Composite Structures, School of Physical Science and Technology, Guangxi University, Nanning 530004, China;* orcid.org/0000-0002-2281-2689; Email: miaolei@gxu.edu.cn

Authors

Jing Peng − *School of Materials Science and Engineering, Anhui University, Hefei 230601, China;* orcid.org/0009-0007-2682-9799

Yang Zhou − *School of Materials Science and Engineering, Anhui University, Hefei 230601, China*

Haoming Xie − *School of Materials Science and Engineering, Anhui University, Hefei 230601, China*

Ru Xia − *Key Laboratory of Environment-Friendly Polymeric Materials of Anhui Province, School of Chemistry and Chemical Engineering, Anhui University, Hefei 230601, China*

Bin Wu − *Key Laboratory of Environment-Friendly Polymeric Materials of Anhui Province, School of Chemistry and Chemical Engineering, Anhui University, Hefei 230601, China*

Complete contact information is available at: https://pubs.acs.org/10.1021/acsanm.4c07152

Author Contributions

J.P.: Writing−original draft. Y.Z.: Investigation. H.X.: Formal analysis. B.W.: Conceptualization. R.X.: Supervision. J.Q.: Project administration. L.S.: Writing—review. L.M.: Methodology, editing, and review.

Notes

The authors declare no competing financial interest.

■ ACKNOWLEDGMENTS

This work was supported by the National Natural Science Foundation of China (No. 52103295), Higher Education Scientific Research Project of Anhui Province (No. 2024AH050077), and GuangXi Science and Technology Project (No. AA23062070).

■ REFERENCES

(1) Wu, X.; Zhang, X.; Yan, X.; Zhang, C.; Zhang, Y.; Li, P.; Li, N.; Liu, H.; Wang, Z. A review: From the whole process of making thermal conductive polymer, the effective method of improving thermal conductivity. *J. Polym. Sci.* **2024**, *62*, 2410−2442.

(2) Guo, J.; Zhang, C.; Zou, W. Fabrication of electrical and thermal conductive thermoplastic polyurethanes-based nanocomposite with azide polyurethane as interfacial compatibilizer. *J. Appl. Polym. Sci.* **2021**, *138* (10), 49958.

(3) Jin, S. W.; Jin, Y. J.; Choi, Y. J.; Kim, D. B.; Yoon, K. H.; Kim, H. W.; Chung, C. M. Eco-friendly preparation and characterization of highly thermally conductive polyimide/boron nitride composites. *Composites, Part A* **2023**, *166*, 107396.

(4) Park, S. J.; Park, J.; Bang, K. M.; Lee, J. M.; Park, W.; Ziolkowski, P.; Jin, H. Thermoelectric hotspot cooling using thermally conductive fillers. *Appl. Therm. Eng.* **2023**, *232*, 120994.

(5) Xu, X.; Zhou, J.; Chen, J. Thermal Transport in Conductive Polymer−Based Materials. *Adv. Funct. Mater.* **2020**, *30* (8), 1904704.

(6) Grancarić, A. M.; Jerković, I.; Koncar, V.; Cochrane, C.; Kelly, F. M.; Soulat, D.; Legrand, X. Conductive polymers for smart textile applications. *J. Ind. Text.* **2018**, *48* (3), 612−642.

(7) Wu, Y.; Xue, Y.; Qin, S.; Liu, D.; Wang, X.; Hu, X.; Li, J.; Wang, X.; Bando, Y.; Golberg, D.; Wang, X.; Chen, Y.; Lei, W.; Chen, Y.; Gogotsi, Y.; Lei, W. BN Nanosheet/Polymer Films with Highly Anisotropic Thermal Conductivity for Thermal Management Applications. *ACS Appl. Mater.* **2017**, *9* (49), 43163−43170.

(8) Wei, B.; Zhang, L.; Yang, S. Polymer composites with expanded graphite network with superior thermal conductivity and electromagnetic interference shielding performance. *Chem. Eng. J.* **2021**, *404*, 126437.

(9) Dai, W.; Lv, L.; Hou, H.; Yan, Q.; Alam, F. E.; Li, Y.; Zeng, X.; Yu, J.; Wei, Q.; Xu, X.; Wu, J.; Jiang, N.; Du, S.; Sun, R.; Xu, J.; Wong, C. P.; Lin, C. T. A Paper-Like Inorganic Thermal Interface Material Composed of Hierarchically Structured Graphene/Silicon Carbide Nanorods. *ACS Nano* **2019**, *13* (2), 1547.

(10) Zeng, X.; Sun, J.; Yao, Y.; Sun, R.; Xu, J. B.; Wong, C. P. A Combination of Boron Nitride Nanotubes and Cellulose Nanofibers for the Preparation of a Nanocomposite with High Thermal Conductivity. *ACS Nano* **2017**, *11* (5), 5167−5178.

(11) Feng, C. P.; Yang, L. Y.; Yang, J.; Bai, L.; Bao, R. Y.; Liu, Z. Y.; Yang, M. B.; Lan, H. B.; Yang, W. Recent advances in polymer-based thermal interface materials for thermal management: A mini-review. *Compos. Commun.* **2020**, *22*, 100528.

(12) Shahil, K. M. F.; Balandin, A. A. Graphene−Multilayer Graphene Nanocomposites as Highly Efficient Thermal Interface Materials. *Nano Lett.* **2012**, *12* (2), 861−867.

(13) Choy, C. L. Thermal conductivity of polymers. *Polymer* **1977**, *18* (10), 984−1004.

(14) Xu, X.; Chen, J.; Zhou, J.; Li, B. Thermal Conductivity of Polymers and Their Nanocomposites. *Adv. Mater.* **2018**, *30* (17), 1705544.

(15) Krupa, I.; Novák, I.; Chodák, I. Electrically and thermally conductive polyethylene/graphite composites and their mechanical properties. *Synth. Met.* **2004**, *145* (2), 245−252.

(16) Han, Z.; Fina, A. Thermal conductivity of carbon nanotubes and their polymer nanocomposites: A review. *Prog. Polym. Sci.* **2011**, *36* (7), 914−944.

(17) Kim, C. B.; Lee, J.; Cho, J.; Goh, M. Thermal conductivity enhancement of reduced graphene oxide via chemical defect healing for efficient heat dissipation. *Carbon* **2018**, *139*, 386−392.

(18) Yao, Y.; Zhu, X.; Zeng, X.; Sun, R.; Xu, J. B.; Wong, C. P. Vertically Aligned and Interconnected SiC Nanowire Networks Leading to Significantly Enhanced Thermal Conductivity of Polymer Composites. *ACS Appl. Mater. Interfaces* **2018**, *10* (11), 9669−9678.

(19) Zhang, F.; Ren, D.; Huang, L.; Zhang, Y.; Sun, Y.; Liu, D.; Zhang, Q.; Feng, W.; Zheng, Q. 3D Interconnected Conductive Graphite Nanoplatelet Welded Carbon Nanotube Networks for Stretchable Conductors. *Adv. Funct. Mater.* **2021**, *31* (49), 2107082.

(20) Chen, Q.; Yang, K.; Feng, Y.; Liang, L.; Chi, M.; Zhang, Z.; Chen, X. Recent advances in thermal-conductive insulating polymer composites with various fillers. *Composites, Part A* **2024**, *178*, 107998.

(21) Jin, C.; Wu, Q.; Yang, G.; Zhang, H.; Zhong, Y. Investigation on hybrid nanofluids based on carbon nanotubes filled with metal nanoparticles: Stability, thermal conductivity, and viscosity. *Powder Technol.* **2021**, *389*, 1−10.

(22) Li, X.; Wu, B.; Chen, P.; Xia, R.; Qian, J. Covalently interconnected carbon nanotubes network enhancing thermal conductivity of EP-based composite. *Compos. Commun.* **2023**, *40*, 101591.

(23) Yang, L.; Zhang, L.; Li, C. Bridging boron nitride nanosheets with oriented carbon nanotubes by electrospinning for the fabrication of thermal conductivity enhanced flexible nanocomposites. *Compos. Sci. Technol.* **2020**, *200*, 108429.

(24) Cai, Y.; Yu, H.; Chen, C.; Feng, Y.; Qin, M.; Feng, W. Improved thermal conductivities of vertically aligned carbon nanotube arrays using three-dimensional carbon nanotube networks. *Carbon* **2022**, *196*, 902−912.

(25) Zhang, H.; He, Q.; Yu, H.; Qin, M.; Feng, Y.; Feng, W. Mussel-Inspired Polymer-Based Composites for Efficient Thermal Management in Dry and Underwater Environments. *ACS Nano* **2024**, *18*, 21399.

(26) Cai, Y.; Yu, H.; Chen, C.; Feng, Y.; Qin, M.; Feng, W. Improved thermal conductivities of vertically aligned carbon nanotube arrays using three-dimensional carbon nanotube networks. *Carbon* **2022**, *196*, 902.
(27) Yu, H.; Feng, Y.; Chen, C.; Zhang, Z.; Cai, Y.; Qin, M.; Feng, W. Thermally conductive, self-healing, and elastic Polyimide@ Vertically aligned carbon nanotubes composite as smart thermal interface material. *Carbon* **2021**, *179*, 348−357.
(28) Yu, H.; chen, C.; Sun, J.; Zhang, H.; Feng, Y.; Qin, M.; Feng, W. Highly Thermally Conductive Polymer/Graphene Composites with Rapid Room-Temperature Self-Healing Capacity. *Nano-Micro Lett.* **2022**, *14*, 135.
(29) Yu, H.; Peng, L.; Chen, C.; Qin, M.; Feng, W. Regulatable Orthotropic 3D Hybrid Continuous Carbon Networks for Efficient Bi-Directional Thermal Conduction. *Nano-Micro Lett.* **2024**, *16*, 198.
(30) Sun, Z.; Yu, H.; Chen, C.; Qin, M.; Feng, W. Core-sheath smart polymer fiber composites with high elasticity and thermal conductivity. *Compos. Sci. Technol.* **2024**, *252*, 110610.
(31) Yu, H.; Feng, Y.; Chen, C.; Zhang, H.; Peng, L.; Qin, M.; Feng, W. Highly Thermally Conductive Adhesion Elastomer Enhanced by Vertically Aligned Folded Graphene. *Adv. Sci.* **2022**, *9*, 2201331.
(32) Zhu, W.; Hu, N.; Wei, Q.; Zhang, L.; Li, H.; Luo, J.; Lin, C. T.; Ma, L.; Zhou, K.; Yu, Z. Carbon nanotube-Cu foam hybrid reinforcements in composite phase change materials with enhanced thermal conductivity. *Mater. Des.* **2019**, *172*, 107709.
(33) Yang, W.; Wang, Y.; Li, Y.; Gao, C.; Tian, X.; Wu, N.; Geng, Z.; Che, S.; Yang, F.; Li, Y. Three-dimensional skeleton assembled by carbon nanotubes/boron nitride as filler in epoxy for thermal management materials with high thermal conductivity and electrical insulation. *Composites, Part B* **2021**, *224*, 109168.
(34) Tian, R.; Jia, X.; Bai, Y.; Yang, J.; Song, H. Fluorinated Graphene thermally conductive hydrogel with a solid−liquid interpenetrating heat conduction network. *ACS Appl. Mater. Interfaces* **2024**, *16* (1), 1451−1460.
(35) Wang, Z.; Fan, L.; Li, R.; Xu, Y.; Fu, Q. Preparation of polymer composites with high thermal conductivity by constructing a "double thermal conductive network" via electrostatic spinning. *Compos. Commun.* **2022**, *36*, 101371.
(36) Li, P.; Shen, H.; Qian, Z.; Yang, X.; Zhao, N.; Zhu, G.; Xu, J. Facile fabrication of flexible layered GO/BNNS composite films with high thermal conductivity. *J. Mater. Sci.* **2018**, *53* (6), 4189−4198.
(37) Jiao, T.; Han, B.; Zhao, L.; Zhang, Z.; Zeng, Y.; Li, D.; Zhang, K.; Deng, Q.; Zhao, Y.; Li, Z. Pie-rolling-inspired construction of vertical carbon fiber high thermal conductivity hybrid networks. *Appl. Surf. Sci.* **2023**, *618*, 156711.
(38) Wu, M.; Yong, S.; Jing, L.; Hou, B.; Li, X.; Zhang, Y.; Yue, J.; Jiang, M.; Sheng, L. Nitrogen-doped porous carbon composite with three-dimensional conducting network for high rate supercapacitors. *J. Alloys Compd.* **2020**, *844*, 156217.

https://doi.org/10.1021/acsanm.4c07152
ACS Appl. Nano Mater. 2025, 8, 3219−3226